Nanoscale

Accepted Manuscript

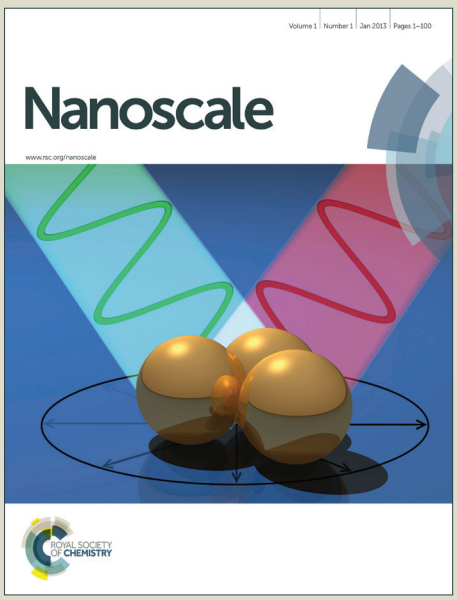

ROYAL SOCIETY OF CHEMISTRY

www.rsc.org/nanoscale

Journal Name

RSCPublishing

ARTICLE

Confining Pt Nanoparticles in Porous Carbon Structure for achieving Durable Electrochemical Performance

Cite this: DOI: 10.1039/xoxxoooooox

Received ooth January 2012,
Accepted ooth January 2012

DOI: 10.1039/xoxxoooooox

www.rsc.org/

C. Yang,[a*] M. Zhou [a] and Q. Xu [b*]

Carbon-supported Pt catalysts have been widely employed as electrocatalysts for energy storage/conversion applications, but have encountered challenging instability issues. In this work, we investigated the degradation behaviors of pore-confined and surface-located Pt nanocatalsyts, employing hollow porous carbon spheres with precisely controlled structure as catalyst support. It is found that by uniformly confining Pt nanoparticles in porous carbon structure, remarkably improved stability and long-term performance of Pt electrocatalysts can be achieved. The nanopore-confined Pt exhibits high retention ratios on both ECSA (54%) and electrocatalytic activity after accelerated degradation tests (ADTs), both of which are almost twice higher than that of the surface-located ones. TEM analysis of the degraded electrocatalysts further revealed that the pore-confinement effect can significantly suppress the Pt degradation processes, including particle migration/agglomeration and detachment from carbon support.

Introduction

Due to the wide applications in fuel cells, biosensors, Li-oxygen/air batteries and etc., Pt-based electrocatalysts have attracted extensive research interests and considerable improvements in catalytic activity have been achieved in the past decade.[1] A lot of research efforts have been focused on the development of more active electrocatalysts while at the same time decreases the required amount of Pt.[2-5] Since Ryoo *et al.*[6] first employed CMK-5 as catalyst support and demonstrated high catalytic activity, mesostructured carbon materials have been widely employed in Pt electrocatalysts due to their desirable properties including high surface area and large pore volume, good conductivity and enhanced mass transport.[7, 8] Yu's group further demonstrated that carbon spheres with hollow core-mesopores shell (HCMS) structure can be a promising supporting material for enhancing the catalytic activity of the supported Pt catalysts.[9-12] Their unique 3D-interconnected hierarchical structures allows efficient mass transport through the macropores/mesopores and increased specific surface area on the level of fine pore systems through mesopores/micropores.[13, 14]

However, the deficiency in long-term durability of Pt and Pt-alloy electrocatalysts still remains as a major challenge for practical applications.[1, 15-18] Nanosized Pt particles tend to grow into large crystallites over time through Ostwald ripening, with surface Pt atoms in small Pt particles dissolve in electrolyte forming cationic Pt species that are subsequently deposit onto large metal particles. Under very severe conditions, such as the cathode of fuel cells, Pt particles can easily migrate on carbon support and subsequently agglomerate. Besides, Pt dissolution occurs at high voltages, especially at start-stop conditions, which can redeposit in the polymer electrolyte membranes and result in a decrease of proton conductivity.[19-21] Degradation of Pt catalysts over time results in gradual loss of electrochemical surface area (ECSA) and a decline in catalytic performance.[18, 22, 23] Thus, in order to improve the long-term performance, the degradation processes of Pt NPs, including particle migration, agglomeration and Pt dissolution, should be suppressed.

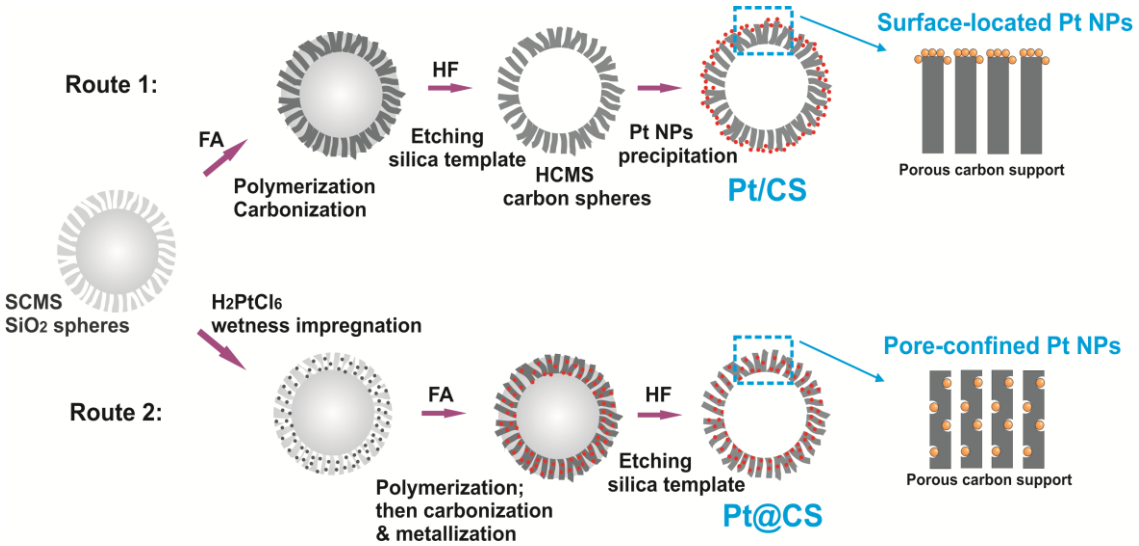

Fig. 1 Schematic synthetic procedures for Pt nanoparticles supported on HCMS carbon spheres: Route 1 shows the widely used 'polyol' method which results in surface-located Pt catalyst (denoted as Pt/CS), and Route 2 is a simply modified procedure which provides pore-confined Pt catalyst (denoted as Pt@CS).

Recent studies have demonstrated that Pt-based electrocatalysts can be stabilized by steric effect via pore confinement/encapsulation.[24, 25] Maiyalagan et al.[26] dispersed Pt and PtRu NPs into 3D bicontinuous interpenetrating channels of highly ordered mesoporous carbon CMK-8 and observed outstanding specific mass activity and superior stability. Galeano et al.[25] confined Pt NPs in nanopores of a mesostructured graphitic carbon support via incipient wetness impregnation method and obtained both improved thermal stability and electrochemical stability. These studies revealed that dispersing Pt NPs into the pore channels of mesostructured carbon support can largely benefit from the pore-confinement effect and remarkably improve the catalyst stability. However, the degradation behaviors of pore-confined Pt catalysts, including particle agglomeration, detachment, and support corrosion, which might be quite different from those surface-located Pt nanocatalysts, haven't been well studied yet. Comparing the degradation behaviors between pore-confined and surface-located Pt NPs is significant for understanding the nanopore-confinement effect toward the Pt degradation mechanisms and will benefit for the design and development of durable Pt-based electrocatalysts. It is worth noting that a rational comparison requires employing the 'same' carbon support with precisely controlled structure and porosity to exclude the possible contribution arising from the porous carbon support.

Herein, we employed the hollow core-mesoporous shell (HCMS) carbon spheres as carbon support and synthesized Pt catalysts with distinct ways of particle depositions via two separate synthetic approaches. Fig. 1 illustrates the synthetic procedures and the structural features of the resulting carbon-supported Pt catalysts. Route 1 shows the synthesis of widely adopted 'polyol' method which results in surface-located Pt catalysts (denoted as Pt/CS), and Route 2 is a simply modified procedure but can provide more uniform dispersion and confinement of Pt NPs throughout the carbon texture (denoted as Pt@CS). Investigation of the degradation behaviors of these two Pt catalysts during the long-term electrochemical operations can give rise to significant insights into the degradation mechanisms at nano-scale occurring on carbon-supported Pt NPs. The contrast morphologies of the catalysts based on the transmission electron microscopy (TEM) analysis before and after the degradation tests provide direct visual proof of the nanopore-confinement effect toward the electrochemical stability of Pt catalysts. The results presented in this work will benefit the design and fabrication of advanced noble metal-based nanocatalysts with optimum catalytic activity and stability for a variety of electrochemical applications.

Experimental section

Synthesis of Pt@CS electrocatalysts

A so-called 'double solvents approach' was employed here, which can effectively impregnate Pt source into the nanopores of the hard templates.[27, 28] Solid core-mesoporous shell (SCMS) silica spheres (core diameter, 300 nm; shell thickness, 80 nm, seeing Supporting Information) (0.6 g) was suspended in dry CH_2Cl_2 (80 ml), to which an aqueous $H_2PtCl_6 \cdot xH_2O$ solution (0.28 ml) containing 8.84 mg Pt was added dropwise under continuous vigorous stirring. The small amount of aqueous H_2PtCl_6 was soaked into hydrophilic pores by capillary force, which greatly minimizes the deposition of H_2PtCl_6 on the outer surface of the silica template. After careful filtration, the yellow powder was collected and dried in vacuum oven at 60 °C overnight. Furfuryl alcohol (0.28 ml) was impregnated into the $H_2PtCl_6 \cdot xH_2O$/SCMS silica composite stored in a refrigerator. The as-synthesized composites were kept at 80 °C for 3 hrs and then 160 °C for 3 hrs in air, then carbonized in a tube furnace at

750 °C for 3 hrs under argon atmosphere. H_2PtCl_6 not only provides the source of Pt but also initiates the polymerization of furfuryl alcohol. The polymerized furfuryl alcohol surrounded the H_2PtCl_6 NPs in the pore space of the silica shells, serving as a protecting agent to prevent the agglomeration of Pt NPs in the subsequent carbonization process.[29] Finally, the silica spheres were etched by 5 wt. % hydrofluoric acid. The obtained Pt catalysts were washed by deionized water and ethanol repeatedly for 5 times and dried at 60 °C in a vacuum oven overnight.

Synthesis of HCMS carbon spheres

HCMS carbon spheres (used as carbon support for Pt/CS catalyst) were synthesized by a nanocasting strategy using SCMS silica spheres (core diameter, 300 nm; shell thickness, 80 nm) as hard template. A solution of furfuryl alcohol (0.28 ml) containing oxalic acid as catalyst with a molar ratio of 30:1 were filled to SCMS silica spheres (0.6 g) by incipient-wetness impregnation method. The composites were kept at 80 °C and then 160 °C for 3 hours in air for polymerization of furfuryl alcohol, then in a tube furnace at 750 °C for 3 hrs under argon atmosphere for carbonization. SiO_2 templates were etched from the silica/carbon composites using 10 wt.% hydrofluoric acid (HF) solution. The obtained carbon spheres were further washed by water and ethanol thoroughly and dried in oven.

Synthesis of Pt/CS electrocatalysts

The surface-located Pt catalyst (Pt/CS) is synthesized by the widely adopted 'polyol' method.[30-32] Pt colloidal solution was prepared first. Chloroplatinic acid hydrate (Pt ~38%) (0.1 g) was dissolved in ethylene glycol (30 ml). The pH was adjusted to 11 by adding 0.5 M NaOH dissolved in ethylene glycol. The above mixture was then heated in oil bath to 140 °C for 4 hours. 2 ml of the obtained Pt colloidal solution was mixed with the above prepared HCMS carbon spheres (200 mg), using HCl solution (0.1 M) to adjust the pH to 5. After stirring overnight at room temperature (25 °C), the products were collected by centrifugation and washed thoroughly by deionized water and ethanol repeatedly. Finally, the obtained catalysts were dried at 60 °C in an oven overnight.

Characterizations

Scanning transmission electron microscopy (STEM, Philips TECNAI 20 with a 200 kV accelerating voltage) and field emission scanning electron microscopy (SEM, Hitachi S-4800 FEG) were used to characterize the morphologies and structures of the as-synthesized SCMS SiO_2 spheres and Pt catalysts. To reveal the exact confinement of Pt NPs within the mesoporous carbon structure, TEM were performed on specially prepared cross-sections of the catalysts as follows: the powder sample was mixed with epoxy and sandwiched between two pieces of silicon wafers. After the epoxy was cured, the assembly was polished own to ~30 mm in thickness and mounted on a standard copper ring for TEM. The whole unit was then ion-milled with the Low Angle Ion Milling & Polishing System 1010 by Fischione Instruments in rocking mode. After a hole was formed at the center of the slit, which held the sample catalysts, extremely thin regions of interest near the edge of the hole were analyzed by TEM.

Raman spectroscopy was carried out on Renishaw Invia Raman Microscope (Renishaw, UK) with He-Ne laser (633 nm, 25 mW). Thermo-gravimmetric analyses (TGA) were performed in air on PERKIN ELMER TGA-7 Thermogravimetric Analyzer to determine the Pt loading. Nitrogen sorption isotherms were obtained on a Micromeritics ASAP 2020 analyzer. The surface area was determined by the Brunauer-Emmett-Teller (BET) method and the pore size distribution was calculated by the Barrett-Joyner-Halenda (BJH) method.

Electrochemical measurements

Electrochemical measurements were conducted on a Solatron SI1287 potentiostat. A three-electrode electrochemical cell was used with Pt plate as counter electrode, Ag/AgCl as reference electrode, and glassy carbon (GC) electrode (from Pine Instruments) with an area of 0.196 cm^2 as working electrode. The GC electrode was polished to a mirror finish using a 0.05 μm Al_2O_3 suspension before experiment. Then 5.0 mg Pt-based catalyst was dispersed by ultrasonication into 800 μL ethanol, 100 μL H_2O, and 100 μL 0.5 wt% Nafion solution. 20 μL of this catalyst ink was pipetted onto the GC electrode and dried at 60 °C for 30 minutes. All electrochemical experiments were performed at room temperature of 22 °C.

The stabilities of the prepared Pt catalysts were investigated by accelerated degradation tests (ADTs), in which, 2000 cyclic potential sweeps were performed in 0.5 M N_2-saturated H_2SO_4 electrolyte in the potential range of 0 - 1.1 V (vs. NHE) at a scan rate of 20 mV s^{-1}. After 20 cycles of cyclic potential sweeps for activation, the CV curves were recorded every 100 cycles to calculate the electrochemical surface area (ECSA) of

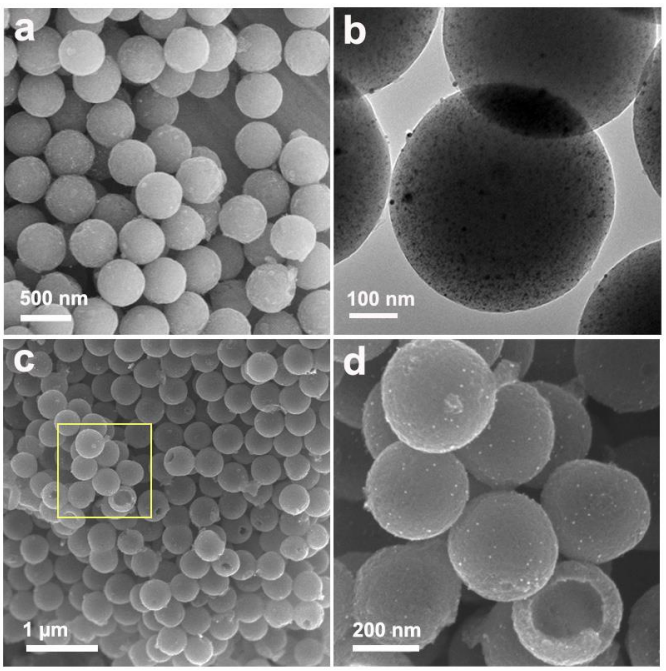

Fig. 2 SEM (a) and TEM (b) images of Pt/carbon/SiO_2 spheres after the carbonization of poly-(furfuryl alcohol) protected SiO_2 spheres with Pt filling in the porous shells. SEM images (c-d) of the Pt@CS catalyst after removing the silica template by HF treatment.

Pt. The catalytic activities for methanol oxidation reaction (MOR) of the examined Pt catalysts were measured before and after the ADT tests in 0.5 M H_2SO_4 containing 1.0 M methanol at a scan rate of 20 mV s^{-1}.

Results and discussion

Characterization of the Pt catalysts

Uniformly confining Pt NPs inside carbon texture with controlled particle size is a challenging task. Therefore, the synthetic process of the Pt@CS catalyst was carefully monitored by TEM and SEM (as shown in Fig. 2) to ascertain the uniform distribution and pore-confinement of Pt NPs. From Fig. 2a, isolated silica spheres can be identified, indicating that both of the poly-(furfuryl alcohol) and hydroplatinic acid were filled into the mesopores of core-shell SiO_2 spheres, instead of depositing on the external surface or in the interstitial spaces between silica spheres. The TEM image (Fig. 2b) clearly revealed that small Pt NPs were well distributed and encapsulated inside the mesoporous shell regions of the SiO_2 spheres without depositing on the external surface or agglomerating into big particles. Considering that these Pt/carbon/silica nanocomposites had been thermally treated at 750 °C for 3 hours, the small and uniform sizes of these Pt NPs imply that the poly(furfuryl alcohol) has provided good protection for Pt NPs during the annealing process. After removing the silica template, the SEM image (Fig. 2c-d) shows that these Pt-impregnated HCMS carbon spheres were isolated, with uniform size and piled up, creating a three dimensional hierarchical structure. More importantly, agglomerations of Pt particles were hardly observed on carbon surface. Since the Pt@CS catalyst has been thermally treated at high temperature, the superior thermal stability suggests that the confinement of Pt NPs in carbon structure may induce some interesting electrochemical properties to the catalyst.

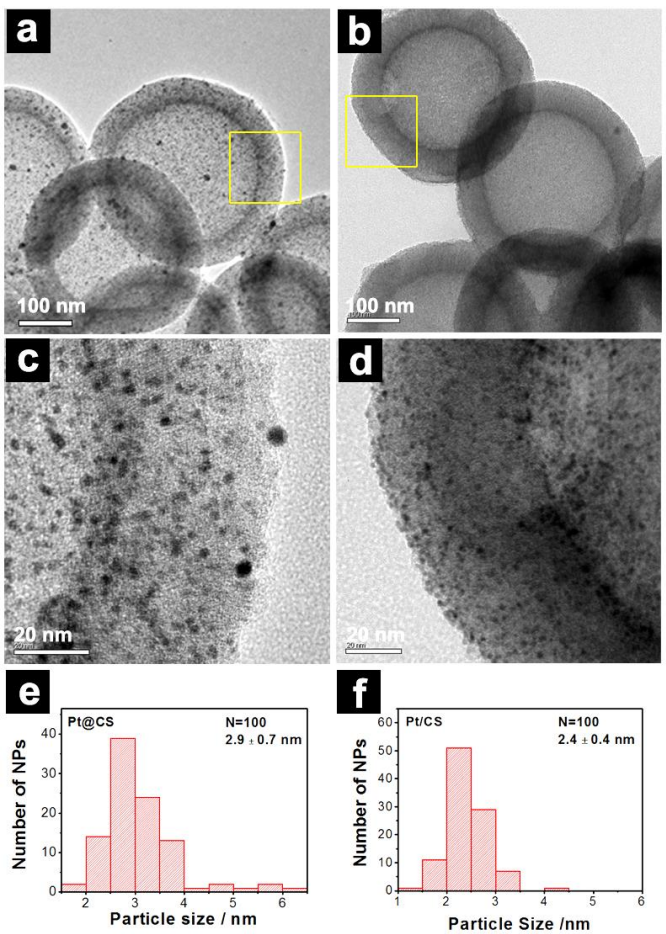

Fig. 3 TEM images of the synthesized Pt catalysts supported on HCMS carbon spheres: (a, c) Pt@CS with Pt NPs confined in the mesoporous carbon shells; (b, d) Pt/CS synthesized by the 'polyol' method with surface-located Pt NPs. (c)and (d) are the high-magnification TEM images of the highlighted area in (a) and (b), respectively. Pt Particle size distribution profiles of Pt@CS (e) and Pt/CS (f).

TEM images of the core/shell section of the HCMS carbon spheres (Fig. 3) clearly reveal the structural features of the Pt@CS and Pt/CS catalysts. It is noticed that uniform dispersion and confinement of Pt NPs in the mesoporous shell regions were achieved on the Pt@CS sample, with only a few Pt particles of <5 nm deposited on the outer carbon surface. On the contrary, a lot of Pt NPs were observed depositing on the external carbon shells in the Pt/CS catalyst. TEM characterization on the commercial E-TEK catalyst (Fig. S1) also reveals that the dispersion of Pt metal catalysts were also limited to the outer surface of Vulcan carbon support, similar to the Pt/CS sample. Particle sizes of 100 Pt particles were measured from the high-magnification TEM images for each sample at randomly selected locations and the size distribution profiles were plotted in Fig. 3e-f. In particular, Pt@CS shows an average Pt particle size of ca. 3-4 nm, whereas the Pt/CS catalyst has relatively small particle size of Pt (ca. 2.4 nm). Structure parameters of the HCMS carbon support, including the hollow core diameter (*D*), mesoporous shell thickness (*S*), were measured from TEM images and summarized in Table 1.

In order to further examine the dispersion of Pt NPs on HCMS carbon spheres, the cross-section of Pt@CS and Pt/CS electrocatalysts were studied by TEM. As shown in Fig. 4a, all Pt NPs were distributed homogeneously across and embedded within the carbon shell regions of Pt@CS. Moreover, no agglomeration of large Pt particles was observed. Whereas most Pt NPs were deposited on either side of the shell region – i.e. inside the macro hollow core (due to the breakage of carbon spheres), or on the external surfaces of the HCMS carbon spheres in Pt/CS.

The N_2 sorption isotherms and corresponding pore size distribution curves of the Pt catalysts supported on HCMS carbon spheres are shown in Fig. 5. Both showed typical type IV hysteresis, suggesting abundant mesoporous pores in the carbon structure. A steep adsorption which occurred around the relative pressure of 0.9-1.0, could be assigned to the existence of hollow macropores. More importantly, a sharp

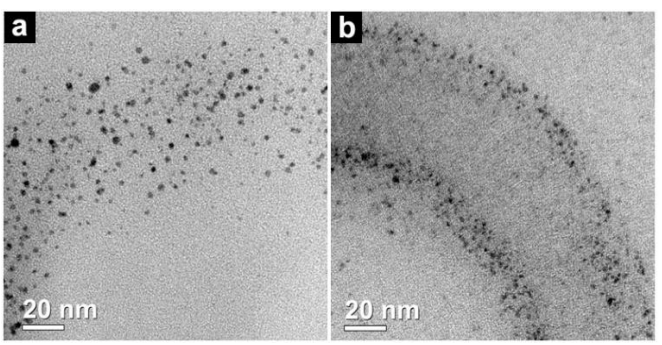

Fig. 4 TEM images of the ¼ region of the cross-sections of the synthesized Pt catalysts supported on the HCMS carbon spheres: (a) Pt@CS and (b) Pt/CS.

Table 1. Structural parameter of the as-synthesized Pt catalysts supported on HCMS carbon spheres.

Samples	D / nm	S / nm	Particle size / nm	Pt wt. %	S_{BET} / $m^2 g^{-1}$	V_p / $m^3 g^{-1}$	d_P / nm
Pt@CS	263 ± 15	52 ± 3	2.9	11.3	1072.5	0.81	3.9
Pt/CS	257 ± 14	54 ± 3	2.4	9.9	1145.3	0.77	3.8

Note: D: Diameter of the macroporous hollow cores of the HCMS carbon spheres; *S*: mesoprous shell thickness of the carbon spheres; Particle size of Pt is measured from the high-magnification TEM images; Pt mass loading (wt. %) is measured by TGA; S_{BET}: BET surface area measured from the N_2 sorption isotherms; V_p: pore volume; D_p: average pore diameter calculated by the BJH method from the N_2 sorption isotherms.

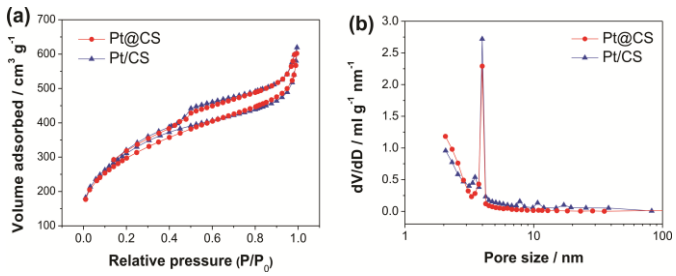

Fig. 5 N_2 sorption isotherms (a) and pore size distribution (b) profiles of the synthesized Pt catalysts supported on HCMS carbon spheres.

characterization peak at 3.8~3.9 nm can be identified from both of samples, indicating uniform mesopore channels with similar pore size were formed in the shell region from its silica template replica. As to the specific surface area, both of the Pt@CS and Pt/CS catalysts provided high surface area of above 1000 $m^2 g^{-1}$.

The amount of graphitization of the synthesized Pt@CS and Pt/CS catalysts was characterized by Raman spectroscopy (Fig. S2). The intensity ratios between the D-band and G-band (I_D/I_G), which reflected the ratio of the amorphous to graphitic carbon content, suggested a similar hydrophilic/hydrophobic character of the HCMS carbon support.

ECSA measurement

The electrochemically active surface areas (ECSA) of these Pt catalysts were firstly estimated from the hydrogen-desorption region of the CV (Fig. S3). A couple of redox peaks, appearing between 0.4V and 0.6V in CV curves of all Pt/CS catalysts, are due to the redox of oxygen-containing functional groups on the surface of carbon support, such as carboxylic, phenolic hydroxyls, or carbonyls.[33-36] The ECSA of Pt@CS and Pt/CS are calculated to be 64 and 81 $m^2 g^{-1}$-Pt, respectively, suggesting that Pt NPs in the Pt@CS sample were not fully exposed due to the pore-confinement by the carbon structure. However, it should be noted that the ECSA of Pt@CS is comparable to that of the commercial E-TEK catalyst (69 $m^2 g^{-1}$-Pt), indicating that the partial encapsulation of Pt NPs inside the mesoporous carbon texture would not limit electrolyte access to Pt surface. The estimated ECSAs in this work agreed to the typical standard values reported in literature[29, 37]

Accelerated degradation tests (ADTs)

The durability of the Pt catalysts were studied by ADTs. The evolution of CV curves over 2000 cycles of ADTs is shown in Fig. 6a-c. The $ECSA_x$ values of Pt for each catalyst after given number of potential cycles (x represents the cycle number) as a percentage of initial ECSA ($ECSA_I$) were then calculated and plotted *against* the degradation cycle in Fig. 6d. Pt@CS outperformed the Pt/CS and E-TEK Pt/VC catalysts). Severe losses of ECSAs (~ 50%) can be observed from the initial 300 potential cycles for both Pt/CS and Pt/VC. On the contrary, the pore-confined Pt@CS catalyst suffered small decay in ECSA, maintained over 70% of the initial ECSA up to 500 repeated potential cycles. With ADTs between 500 to 2000 cycles, the degradation curves for all catalysts gradually stabilize and decay at similar rate. After 2000 repeated potential cycles, Pt@CS retained an ECSA of above 50%, almost twice higher than that of the Pt/CS (29%) and the E-TEK Pt/VC (21%) catalysts. The evolution of ECSAs clearly revealed that the Pt NPs uniformly dispersed in carbon nanopores can deliver remarkable electrochemical stabilities with well-maintained ECSA after long-term operations.

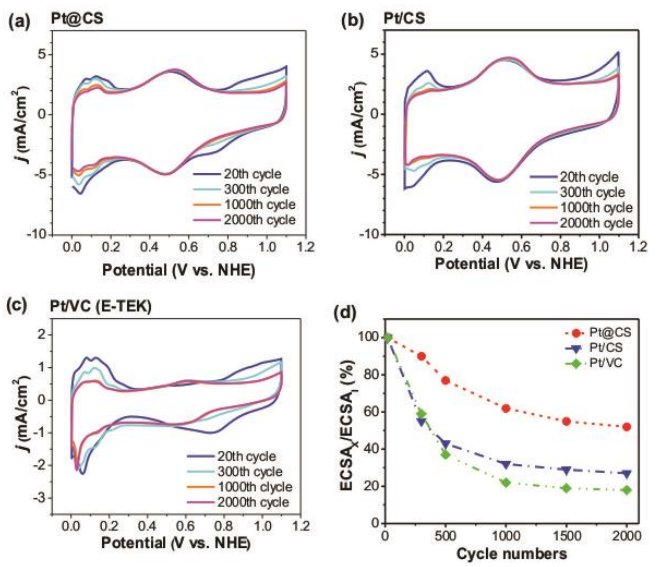

Fig. 6 The 20th, 300th, 1000th and 2000th CV curves of (a) Pt@CS, (b) Pt/CS, and (c) the E-TEK Pt/VC (10 wt.%) catalyst in 0.5 M N_2-saturated H_2SO_4 electrolytes scanned in the potential range of 0 – 1.1 V (vs. NHE) at a scan rate of 20 mV s^{-1}. (d) The ECSA retention ratio as a function of cycle numbers during the degradation tests. ($ECSA_I$ is the initial Pt surface area measured before the degradation potential cycles.)

Characterization of degraded Pt catalysts

In order to understand the underlying reasons for the enhanced electrochemical stability of the nanopore-confined Pt catalyst, the morphology of all degraded Pt catalysts after the 2000 ADTs in H_2SO_4 electrolyte were characterized by TEM. As shown in Fig. 7, although both of the Pt@CS and Pt/CS catalysts can maintain the core-shell carbon structure, Pt morphologies are quite different. In the degraded Pt@CS sample, we can still find a relative large amount of Pt NPs evenly distributed in the shell regions. The degradation process caused a small loss in the total metal particle numbers. From the higher magnification TEM images, some smaller Pt particles (< 2 nm in diameter) were observed as indicated by blue arrows. A few large Pt particles with a diameter of 5-15 nm also appeared as indicated by dashed circles. On the contrary, the degradation and mobility of Pt NPs in the Pt/CS and Pt/VC catalysts are more pronounced: severe particle growth occurred as big agglomeration of Pt particles with diameter of >50 nm can be easily identified in Fig. 7c and d; nevertheless, the numbers of Pt particles were remarkably decreased. It is therefore concluded that the large amount of small Pt NPs trapped inside mesoporous carbon structures which are well-maintained during the ADTs, lead to the high retention ratio of ECSA for Pt@CS. Considering that both Pt@CS and Pt/CS are supported on the same HCMS carbon spheres, these TEM observations thus provide conclusive proof for the enhanced electrochemical stability of the pore-confined Pt NPs.

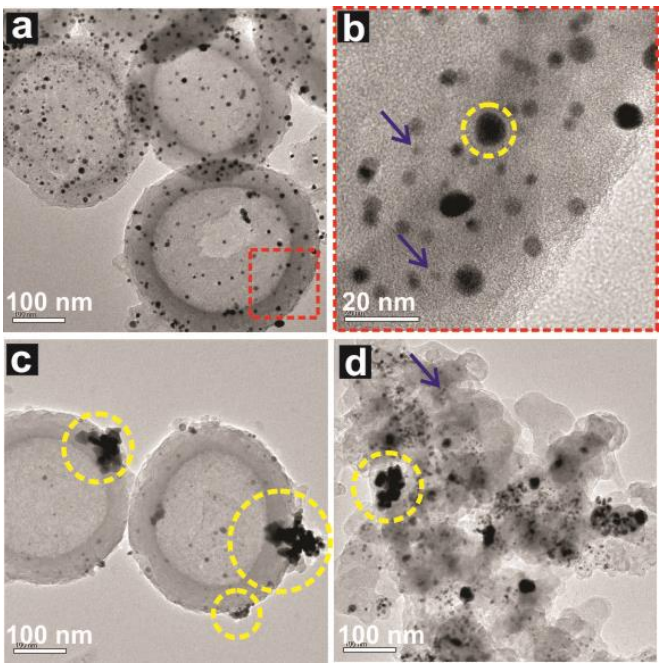

Fig. 7 TEM images of the degraded catalysts after 2000 cycles of ADTs: (a-b) Pt@CS. (b) is the high-magnification TEM image of the highlighted area in (a). The blue arrows points at Pt NPs with reduced particle size and the dashed yellow cycle indicates enlarged Pt NPs; (c) Pt/CS and (d) Pt/VC. The dashed circles highlight agglomerated Pt particles.

Discussions

Designing effective strategies to mitigate the catalyst degradation requires a deep understanding of the underlying mechanisms. According to the degradation mechanisms that have been proposed in literature, four processes are considered to be responsible for the decay of Pt electrocatalysts:[18, 22, 23, 38-40] (1) Pt particle growth via *Ostwald Ripening* effect, (2) Pt crystal migration and coalescence, (3) dissolution and reprecipitation of Pt in ion conductor, and (4) detachment of Pt nanoparticles (NPs) from carbon support. It is generally accepted that these degradation mechanisms that occur on Pt catalysts are closely related to the structure and morphology of the catalysts.

Since the carbon supports of both Pt@CS and Pt/CS catalysts possessed similar structural features and porosities due to the replication from the same silica template, the enhancement of the catalytic durability arising from the contribution of the porous carbon support can be excluded. Confining Pt NPs in porous carbon structure is therefore believed to be the key contributor for enhancing the durability of the Pt@CS electrocatalyst. The uniform dispersion and confinement of Pt NPs in porous carbon structure make metal NPs well separated and less prone to the Oswald Ripening effect. Moreover, due to the 3D restriction from the carbon wall, degradation mechanisms such as particle detachment from carbon support, particle agglomeration due to Pt crystal migration and coalescence, have also being effectively suppressed. As shown in Fig. 7b, the maintained Pt NPs in the degraded Pt@CS electrocatalyst are found with bimodal particle sizes. According to the dissolution/re-deposition degradation mechanism[41], it is possible that the oxidized Pt species were trapped inside the porous carbon channels, and quickly redeposit on the nearby Pt NPs. Therefore, the hierarchical structure of the HCMS carbon spheres creates a complicated three-dimensional porous network, which can significantly increase the probability for successful re-adsorption/reduction of dissolved Pt species, thus in turn leads to an improved retention of ECSA and catalytic activity.

On the contrary, although the as-prepared Pt/CS catalyst is supported on the same HCMS carbon support and demonstrated promising initial catalytic activity (methanol oxidation reaction was used to identify the catalytic activity of these Pt catalysts, as seen in Supporting Information Fig. S4), the long-term electrochemical stability is still a problem. The surface-located Pt NPs, as in case of the Pt/CS and E-TEK catalysts, create higher local current 'hot spots' during the electrocatalytic reations, which are conducive to sintering and promote the degradation processes such as the particle agglomeration via Ostwald Ripening effect, the Pt crystal migration and coalescence, as well as particle detachment. As a result, the ECSA and catalytic activity decayed quickly and large agglomerations of Pt particles with particle size up to 100 nm were observed on both of the degraded Pt/CS and E-TEK catalysts.

Conclusions

By specifically modifying the synthetic procedures, we created two Pt catalysts supported on the 'identical' mesostructured carbon support with well-controlled structural parameters and hierarchy of porosities but distinct ways of particle depositions. The Pt@CS catalyst uniformly confines Pt NPs in the porous structure of the carbon support, whereas the Pt/CS catalyst prepared via the 'polyol' method and the commercial E-TEK Pt/VC catalysts have Pt NPs located on the external carbon surface fully exposed to the electrolyte.

We further investigated the degradation behaviors of the pore-confined Pt catalysts (Pt@CS) and compared with that of surface-located Pt catalysts (Pt/CS). Results show that the pore-confined Pt catalysts benefits the achievement of high stability and demonstrates high retention ratio of both ECSA and electrocatalytic activity for almost twice higher than that of the surface-located Pt catalysts. Morphology of the degraded Pt catalysts analyzed by TEM reveals that the pore-confinement effect can effectively mitigated the Pt degradation processes including particle agglomeration, migration, and dissolution, therefore play an important role in the enhancement of durability of Pt-based electrocatalysts. The presented work would benefit the design and development of other advanced heterogeneous electrocatalysts with optimum catalytic activity and durability.

Acknowledgements

Dr. C. Yang thanks Prof. Kwong-Yu Chan for the helpful discussion and EMU, The University of Hong Kong for their help on materials characterizations. Dr. Q. Xu thanks the supports by a grant from the NSFC, China (Project No. 51306076) and a New Faculty Grant from Jiangsu University, China (Project No. 1291130022).

Notes and references

[a] Department of Chemistry, The University of Hong Kong, Pokfulam Road, Hong Kong S.A.R.
Current address: Rm 631, Main Research Building, 2-1, Hirosawa, Wako, Saitama 351-0198, Japan
Address correspondence to chunzhenxp@gmail.com
[b] School of Energy and Power Engineering, Jiangsu University, Zhenjiang, P.R. China
Address correspondence to hawkingxq@hotmail.com

1. X. Zhao, M. Yin, L. Ma, L. Liang, C. P. Liu, J. H. Liao, T. H. Lu and W. Xing, *Energ Environ Sci*, 2011, **4**, 2736-2753.
2. K. Sasaki, H. Naohara, Y. Choi, Y. Cai, W. F. Chen, P. Liu and R. R. Adzic, *Nat Commun*, 2012, **3**, 1115.
3. X. Cui, J. Shi, Y. Wang, Y. Chen, L. Zhang and Z. Hua, *ChemSusChem*, 2014, **7**, 135-145.
4. R. Wang, Y. Xie, K. Shi, J. Wang, C. Tian, P. Shen and H. Fu, *Chemistry - A European Journal*, 2012, **18**, 7443-7451.
5. L. Wang, C. Tian, H. Wang, Y. Ma, B. Wang and H. Fu, *The Journal of Physical Chemistry C*, 2010, **114**, 8727-8733.
6. S. H. Joo, S. J. Choi, I. Oh, J. Kwak, Z. Liu, O. Terasaki and R. Ryoo, *Nature*, 2001, **412**, 169-172.
7. S. L. Candelaria, Y. Shao, W. Zhou, X. Li, J. Xiao, J.-G. Zhang, Y. Wang, J. Liu, J. Li and G. Cao, *Nano Energy*, 2012, **1**, 195-220.
8. A. S. Arico, P. Bruce, B. Scrosati, J. M. Tarascon and W. Van Schalkwijk, *Nat Mater*, 2005, **4**, 366-377.
9. G. S. Chai, S. B. Yoon, J. H. Kim and J. S. Yu, *Chem Commun*, 2004, 2766-2767.
10. B. Fang, J. H. Kim, M.-S. Kim and J.-S. Yu, *Accounts of chemical research*, 2013, **46**, 1397-1406.
11. B. Fang, M. Kim, J. H. Kim and J.-S. Yu, *Langmuir*, 2008, **24**, 12068-12072.
12. B. Fang, J. H. Kim, M. Kim and J.-S. Yu, *Chem Mater*, 2009, **21**, 789-796.
13. J. Wu, F. P. Hu, X. D. Hu, Z. D. Wei and P. K. Shen, *Electrochim Acta*, 2008, **53**, 8341-8345.
14. L. Wang, C. G. Tian, H. X. Zhang and H. G. Fu, *Eur J Inorg Chem*, 2012, 961-968.
15. H. A. Gasteiger, S. S. Kocha, B. Sompalli and F. T. Wagner, *Appl Catal B-Environ*, 2005, **56**, 9-35.
16. R. Borup, J. Meyers, B. Pivovar, Y. S. Kim, R. Mukundan, N. Garland, D. Myers, M. Wilson, F. Garzon, D. Wood, P. Zelenay, K. More, K. Stroh, T. Zawodzinski, J. Boncella, J. E. McGrath, M. Inaba, K. Miyatake, M. Hori, K. Ota, Z. Ogumi, S. Miyata, A. Nishikata, Z. Siroma, Y. Uchimoto, K. Yasuda, K. Kimijima and N. Iwashita, *Chem Rev*, 2007, **107**, 3904-3951.
17. W. M. Chen, *Prog Chem*, 2012, **24**, 246-252.
18. Y. Shao-Horn, W. C. Sheng, S. Chen, P. J. Ferreira, E. F. Holby and D. Morgan, *Top Catal*, 2007, **46**, 285-305.
19. C. Hartnig and T. J. Schmidt, *J Power Sources*, 2011, **196**, 5564-5572.
20. T. Okada, Y. Ayato, H. Satou, M. Yuasa and I. Sekine, *The Journal of Physical Chemistry B*, 2001, **105**, 6980-6986.
21. E. Guilminot, A. Corcella, F. Charlot, F. Maillard and M. Chatenet, *J Electrochem Soc*, 2007, **154**, B96.
22. J. C. Meier, C. Galeano, I. Katsounaros, A. A. Topalov, A. Kostka, F. Schuth and K. J. J. Mayrhofer, *Acs Catal*, 2012, **2**, 832-843.
23. J. C. Meier, I. Katsounaros, C. Galeano, H. J. Bongard, A. A. Topalov, A. Kostka, A. Karschin, F. Schuth and K. J. J. Mayrhofer, *Energ Environ Sci*, 2012, **5**, 9319-9330.
24. Y. H. Ng, S. Ikeda, T. Harada, T. Sakata, H. Mori, A. Takaoka and M. Matsumura, *Langmuir*, 2008, **24**, 6307-6312.
25. C. Galeano, J. C. Meier, V. Peinecke, H. Bongard, I. Katsounaros, A. A. Topalov, A. H. Lu, K. J. J. Mayrhofer and F. Schuth, *J Am Chem Soc*, 2012, **134**, 20457-20465.
26. T. Maiyalagan, T. O. Alaje and K. Scott, *J Phys Chem C*, 2012, **116**, 2630-2638.
27. X. B. Huang, W. J. Dong, G. Wang, M. Yang, L. Tan, Y. H. Feng and X. X. Zhang, *J Colloid Interf Sci*, 2011, **359**, 40-46.
28. A. Aijaz, A. Karkamkar, Y. J. Choi, N. Tsumori, E. Ronnebro, T. Autrey, H. Shioyama and Q. Xu, *J Am Chem Soc*, 2012, **134**, 13926-13929.
29. F. J. Li, K. Y. Chan and H. Yung, *J Mater Chem*, 2011, **21**, 12139-12144.
30. C. Bock, C. Paquet, M. Couillard, G. A. Botton and B. R. MacDougall, *J Am Chem Soc*, 2004, **126**, 8028-8037.
31. B. L. Cushing, V. L. Kolesnichenko and C. J. O'Connor, *Chem Rev*, 2004, **104**, 3893-3946.
32. Y. Y. Chu, Z. B. Wang, D. M. Gu and G. P. Yin, *J Power Sources*, 2010, **195**, 1799-1804.
33. R. Q. Yu, L. W. Chen, Q. P. Liu, J. Y. Lin, K. L. Tan, S. C. Ng, H. S. O. Chan, G. Q. Xu and T. S. A. Hor, *Chem Mater*, 1998, **10**, 718-722.
34. H. Luo, Z. Shi, N. Li, Z. Gu and Q. Zhuang, *Anal Chem*, 2001, **73**, 915-920.
35. H. P. Boehm, *Carbon*, 1994, **32**, 759-769.
36. K. Esumi, M. Ishigami, A. Nakajima, K. Sawada and H. Honda, *Carbon*, 1996, **34**, 279-281.
37. F. Zaragoza-Martin, D. Sopena-Escario, E. Morallon and C. S. M. de Lecea, *J Power Sources*, 2007, **171**, 302-309.
38. W. M. Chen, G. Q. Sun, Z. X. Liang, Q. Mao, H. Q. Li, G. X. Wang, Q. Xin, H. Chang, C. H. Pak and D. Y. Seung, *J Power Sources*, 2006, **160**, 933-939.
39. P. Joghee, S. Pylypenko, T. Olson, A. Dameron, A. Corpuz, H. N. Dinh, K. Wood, K. O'Neill, K. Hurst, G. Bender, T. Gennett, B.

Pivovar and R. O'Hayre, *J Electrochem Soc*, 2012, **159**, F768-F778.
40. W. C. Sheng, S. Chen, E. Vescovo and Y. Shao-Horn, *J Electrochem Soc*, 2012, **159**, B96-B103.
41. A. Schneider, L. Colmenares, Y. E. Seidel, Z. Jusys, B. Wickman, B. Kasemo and R. J. Behm, *Phys Chem Chem Phys*, 2008, **10**, 1931-1943.